Research Article

Zhenyu Guo, Weiqiang Song*, Xueqin Wei, Yu Feng, Yixuan Song, Zidong Guo, Wenxi Cheng, Wei Miao, Bo Cheng, and Shiping Song

Effect of matrix composition on the performance of calcium carbonate filled poly(lactic acid)/poly (butylene adipate-*co*-terephthalate) composites

https://doi.org/10.1515/epoly-2023-0026
received April 01, 2023; accepted May 22, 2023

Abstract: The ratio of poly(lactic acid) (PLA), poly(butylene adipate-*co*-terephthalate) (PBAT), and calcium carbonate ($CaCO_3$) fillers in PLA/PBAT/$CaCO_3$ composites was set at 90/10/5, 70/30/5, and 30/70/5. The effect of nano- and micro-$CaCO_3$ on the melting and crystallization performance of the composites was investigated by differential scanning calorimetry. PLA crystallization was related to the PLA and PBAT ratio, cooling rate, and $CaCO_3$ particle size in PLA/PBAT/$CaCO_3$ composites. Nano-$CaCO_3$ prevented the crystallization of PLA in PLA/PBAT/$CaCO_3$ 90/10/5 and 70/30/5 but did not prevent the crystallization of PLA in PLA/PBAT/$CaCO_3$ 30/70/5. Unlike nano-$CaCO_3$, micro-$CaCO_3$ did not prevent PLA crystallization regardless of the PLA and PBAT ratio. Nano- and micro-$CaCO_3$ enhance PLA90 and PLA70 to some extent, due to the aggregation and dissociation of the $CaCO_3$ filler in polylactic acid. But nano- and micro-$CaCO_3$ improved the mechanical properties of PLA30 several times, due to the good compatibility of the $CaCO_3$ filler and PBAT. The effect of nano-$CaCO_3$ and micro-$CaCO_3$ on the mechanical properties of PLA/PBAT/$CaCO_3$ composites had no significant difference.

Keywords: poly(lactic acid), poly(butylene adipate-*co*-terephthalate), nano-sized calcium carbonate, micro-sized calcium carbonate, non-isothermal crystallization

*** Corresponding author: Weiqiang Song,** School of Materials Science and Engineering, Henan University of Technology, Zhengzhou 450001, China; Henan Hairuixiang Technology Co., Ltd, Pingdingshan 467100, China, e-mail: weiqiang_song@haut.edu.cn
Zhenyu Guo, Xueqin Wei, Zidong Guo, Wenxi Cheng, Wei Miao, Bo Cheng, Shiping Song: School of Materials Science and Engineering, Henan University of Technology, Zhengzhou 450001, China
Yu Feng: School of Art, Henan University of Technology, Zhengzhou 450001, China
Yixuan Song: School of Art, Shengda Economics Trade and Management College of Zhengzhou, Zhengzhou, Henan 451191, China

1 Introduction

Most of plastic mulches used in agriculture and the packaging materials in supermarkets are non-biodegradable polyethylene, polypropylene, polyvinyl chloride, and other resin-based disposable plastic materials, which are durable, anti-corrosive, and inexpensive plastic based on fossil fuels (1). However, they have the obvious disadvantage of being difficult to degrade in the natural environment. Despite improved end-of-life management of plastics and increasing public awareness of the consequences of improper disposal of plastic waste, nearly half of all non-degradable plastic waste is still not recycled each year due to the relatively high annual economic cost of removal and disposal (2). To address the damage to the environment, there is a strong need to develop biodegradable and compostable plastics.

Biodegradable polymers can be derived from cellulose and starch, or from non-renewable resources such as petroleum. Typical representatives of the former are polylactic acid (PLA) and poly-3-hydroxybutyrate (3), and typical representatives of the latter are poly(butylene adipate-*co*-terephthalate) (PBAT) and polycaprolactone (4). Among these polyesters, the consumption of PLA is the largest, which is mainly used in packaging and biomedical industrial application. However, its brittle nature limits its wider use. Therefore, PLA is usually blended with other degradable polymers to improve toughness (5–7). PBAT, on the other hand, is a very flexible biodegradable polymer, which is most often selected to blend with PLA (8–10). The combination of these two polymers can guarantee good performance in applications, where a homogeneous touch with better toughness can be obtained without reducing tensile properties, transparency, or water vapor barrier (11–13).

The current problem is that the cost of PBAT/PLA blends is higher than traditional non-degradable plastics, which limits their large-scale application. To overcome

this problem, low-cost fillers (e.g., natural fibers (14,15) and common minerals (16–18)) are used. Among the options, calcium carbonate ($CaCO_3$), widely used in plastics, is the preferred one. The combination of PBAT/PLA with $CaCO_3$ not only reduces the cost but also improves the performance of the matrix.

There are two kinds of $CaCO_3$ fillers commonly used, namely nano- and micro-$CaCO_3$. Nano-$CaCO_3$ can improve the rheological property and plasticity of plastic masterbatch in plastics processing and can play a dual role of toughening and strengthening in plastics properties, so that the bending strength, elastic modulus, heat deflection temperature, and dimensional stability of plastics can be improved, and thermal hysteresis can also be given to plastics (19–22). However, due to its large specific surface area and high surface energy, nano-$CaCO_3$ is easily agglomerated, resulting in its enhanced properties not being realized (23–27). It would be too wasteful to use nano-$CaCO_3$ only as a weight-adding agent. Compared to nano-$CaCO_3$, micro-$CaCO_3$ has received less attention. In fact, the surface of micro-$CaCO_3$ particles is in a thermodynamically stable state, unlike nano-$CaCO_3$, which is easy to be dispersed and can achieve the performance of nano-$CaCO_3$ in many plastics. The low cost of production and use of micro-$CaCO_3$ is favorable to further reduce the cost of biodegradable plastics and to increase their market share.

Of course, the performance of the PLA/PBAT/$CaCO_3$ composite depends mainly on the matrix and only secondarily on the filler. However, PLA is poorly compatible with PBAT. When PLA is dominant in the matrix, it forms continuous phase, while PBAT forms dispersed phase, and *vice versa*. The microscopic morphology of the PLA/PBAT blends depended on the relative content of both. As the PBAT content increases from 5 to 50 wt%, PBAT as the dispersed phase gradually transitions from a spherical droplet, elongated fiber structure to a co-continuous structure with PLA. When the PBAT content reached 70 wt% and above in the PLA/PBAT blend, PLA transformed into the dispersed phase (28). The relationship between the morphology and composition of PLA/PBAT blends was inferred in more detail by Deng et al. from various analyses such as melt viscosity, optical micrograph, tensile behavior, and SEM fracture surface (13). PLA/PBAT blends formed a PLA/PBAT co-continuous phase when the PBAT content ranged from 19.0 to 40 wt%. When the PBAT content reached 40 wt% and above, PLA constituted dispersed phase particles dispersed in the PBAT continuous matrix. When the PBAT content was greater than 60 wt%, the PLA particles became finer in size and more uniformly dispersed, and the blend had properties similar to that of the neat PBAT.

On the other hand, the $CaCO_3$ filler has different affinities with PLA and PBAT. The filler tends to disperse preferentially in PBAT. Song had conducted relevant research on the influence of $CaCO_3$ filler on the mechanical and thermal properties of PLA/PBAT composite materials (29). However, Song's research only considered the impact of fillers on the performance, while ignoring the impact of changes in PLA and PBAT content in the matrix on the performance. In the present study, the weight ratio of PLA/PBAT in the composites was set at 90/10, 70/30, and 30/70, which corresponds to three forms of PLA/PBAT/$CaCO_3$ composites, respectively. The effect of the filler on the performance of the PLA/PBAT/$CaCO_3$ composite was revealed.

2 Experimental method

2.1 Materials

PLA (FY801, density: 1.24 g·cm^{-3}, melt mass-flow rate = 4 g per 10 min at 190°C and 2.16 kg) was purchased from Anhui Fengyuan Co. PBAT (blow molding grade) was purchased from Lanshan Tunhe Co. Maleic anhydride grafted polylactic acid (LGM, G1603) was purchased from Foshan Zuogao Plastic Material Co. Micro-$CaCO_3$ and nano-$CaCO_3$ were supplied by Nanzhao Dingcheng Calcium Industry Co. The characteristic parameters of $CaCO_3$ fillers are listed in Table 1.

2.2 Preparation of PLA/PBAT/$CaCO_3$ composites

Prior to mixing, PBAT and PLA were dried in a vacuum oven at 60°C for 12 h to minimize moisture. Subsequently,

Table 1: Particle size and distribution of $CaCO_3$ filler

	Purity (%)	D50	Size distribution	Specific surface area ($m^2 \cdot g^{-1}$)	Activating agent
Nano-$CaCO_3$	≥98.5	65 nm	1.6	34	Stearic acid
Micro-$CaCO_3$	≥98.5	5 μm	2.3	6.2	Stearic acid

they were added to a mechanical mixer. $CaCO_3$ and LGM were then added to the mixture of PBAT and PLA. Sample formulations and corresponding names are provided in Table 2. The melt mixing was carried out in a twin-screw extruder with a screw speed of 60 rpm and a temperature range of 170–190°C.

2.3 Differential scanning calorimetry (DSC)

The thermal transition of PLA/PBAT/$CaCO_3$ composites was investigated using a DSC (DZ-DSC 300, Nanjing Dazhan Testing Instruments Co., Ltd). Both heating and cooling rates were set to 20°C·min^{-1} at 9 ± 1 mg of each sample. The sample was heated from 40°C to 210°C in a nitrogen atmosphere and held for 5 min, then cooled to 40°C. The cooled samples were then reheated to 210°C. Glass transition temperature (T_g), cold crystallization temperature (T_{cc}), enthalpy of cold crystallization (ΔH_{cc}), melting temperature (T_m), and enthalpy of melting (ΔH_m) were obtained from the heating DSC curves. The crystallinity (X_c) was determined from Eq. 1 as follows:

$$X_c = (\Delta H_m - \Delta H_{cc})/(\Delta H_m^0 \cdot w_{PLA}) \times 100\% \quad (1)$$

where ΔH_m^0 = 93.6 J·g^{-1} is for 100% crystalline PLA (7) and w_{PLA} is the mass% of PLA in the sample. The melt crystallization temperature (T_c) and crystallization enthalpy (ΔH_c) were derived from the cooling scans.

2.4 Non-isothermal crystallization kinetics

The samples were heated from 40°C to 210°C at 20°C·min^{-1} and held for 5 min. Subsequently, the samples were cooled to room temperature at −4, −6, −8, and −10°C·min^{-1}, respectively. The crystallization time was converted by Eq. 2 as follows:

$$t = (T_0 - T)/\phi \quad (2)$$

where t is the crystallization time, T_0 is the initial crystallization temperature, T is the temperature at time t, and φ is the cooling rate.

Table 2: Formulations of PLA/PBAT/$CaCO_3$ composites

Sample code	PLA	PBAT	LGM	Nano-$CaCO_3$	Micro-$CaCO_3$
PLA90	90	10	2		
PLA90NC5	90	10	2	5	
PLA90MC5	90	10	2		5
PLA70	70	30	2		
PLA70NC5	70	30	2	5	
PLA70MC5	70	30	2		5
PLA30	30	70	2		
PLA30NC5	30	70	2	5	
PLA30MC5	30	70	2		5

2.5 Tensile testing

Tensile testing was carried out on an electronic universal testing machine (WUW-50H, Jinan Huaxing Testing Equipment Co., Ltd, China) according to GB/T 1040.1-2006. Tensile rate was set at 20 mm·min^{-1}. The test was repeated for five times for each sample and the average value was taken. Testing impact strength was performed on an Izod impact test machine (XJUD-22, Chengde Juyuan Testing Equipment Manufacture Co., Ltd, China) according to GB/T 2611. Impact speed was 3.5 m·s^{-1}. The impact test was repeated five times for each sample and the average value was taken.

2.6 Scanning electron microscopy (SEM)

The morphology of the fracture surfaces of the samples in the tensile testing was recorded by using an SEM (Regulus8100, HITACHI, Japan) under a voltage of 5 kV at 5,000 times magnification. The samples were gold coated before examination.

3 Results and discussion

3.1 Melting and crystallization behaviors in the PLA/PBAT/$CaCO_3$ composites

Nascent PLA/PBAT/$CaCO_3$ composites were investigated by using DSC technology, and the results of the first-heating, cooling, and second-heating DSC scans are shown in Figure 1.

PBAT is a random co-polymer and therefore lacks a sufficiently symmetrical structure, and hence, does not have the ability to give high levels of crystallinity (22). As shown in Figure 1, PBAT had a very broad and shallow endotherm even in PLA30, PLA30NC5, and PLA30MC5, indicating low crystallization. But PLA had obvious

endotherms owing to the cold crystallization, melt crystallization, and melting process as shown in Figure 1 even if the PLA content was as low as 30 parts in PLA30 regardless of whether there was $CaCO_3$ fillers in the study. Moreover, the peaks of melting endotherm and crystallization exotherm attributed to PLA were affected by the PBAT content and particle size of the $CaCO_3$ fillers.

The parameters derived from the first heating DSC scans of the PLA/PBAT/$CaCO_3$ composites are shown in Figure 1b. The melting temperature of PLA (T_{mPLA}) in PLA90 and PLA30 with PLA and PBAT single-continuous phases, respectively, slightly decreased after the addition of $CaCO_3$ fillers, especially decreased substantially, after the addition of micro-$CaCO_3$. But T_{mPLA} in PLA70 with

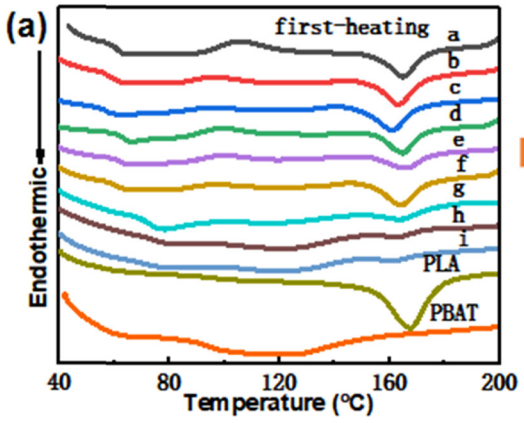

(b)

	T_{ccPLA} (°C)	ΔH_{ccPLA} (J·g^{-1})	X_{ccPLA} (%)	T_{mPBAT} (°C)	T_{mPLA} (°C)	ΔH_{mPLA} (J·g^{-1})	X_{mPLA} (%)
PLA	-	-	-	-	168	16.5	17.6
PBAT				117			
a	106	6.64	8.0	-	165	13.1	15.7
b	96.9	2.73	3.3	-	164	17.2	20.5
c	96.7	1.17	1.4	-	161	13.2	15.8
d	99.8	4.51	6.9	-	165	13.6	20.7
e	101	3.23	4.9	-	167	10.4	15.9
f	97.2	1.34	2.0	-	164	15.5	23.6
g	-			116	164	3.13	34.1
h	-			122	163	1.37	15.7
i	-			121	161	1.23	14.1

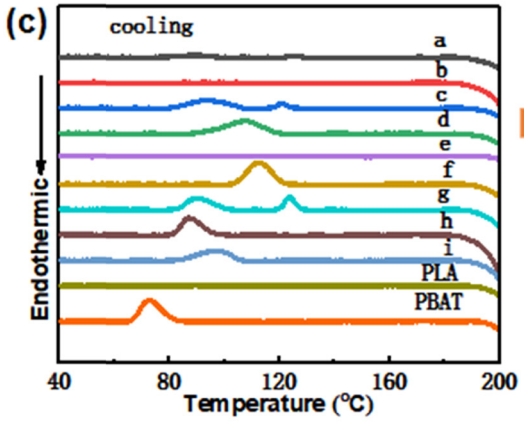

(d)

	T_c (°C)	T_c' (°C)	$t'_{1/2}$ (second)
PLA	-	-	-
PBAT	-	72.9	-
a	126	89.2	40
b	-	-	-
c	124	93.1	44
d	-	108	111
e	-	-	-
f	-	112	49
g	124	90.4	38
h	-	87.5	33
i	-	97.7	41

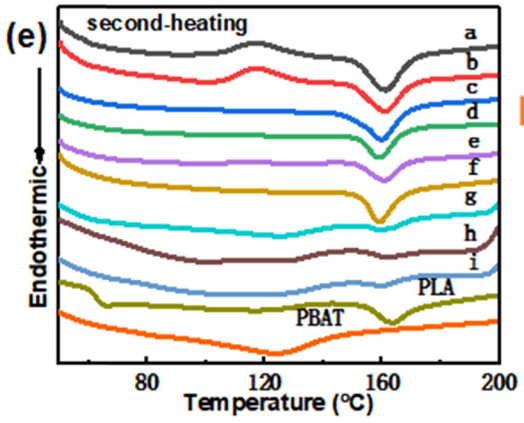

(f)

	T_{ccPLA} (°C)	T_{mPBAT} (°C)	T_{mPLA} (°C)
PLA	-	-	164
PBAT	-	125	
a	117	-	161
b	117	-	161
c	-	-	160
d	-	-	159
e	116	-	161
f	-	-	159
g	-	126	160
h	-	127	163
i	-	126	161

Figure 1: DSC curves and derived parameters of PLA/PBAT/$CaCO_3$ composites at 20°C·min^{-1} for (a and b) first-heating, (c and d) cooling, and (e and f) second-heating. a–i presented in each of the subfigures (a–f) stand for a. PLA90, b. PLA90NC5, c. PLA90MC5, d. PLA70, e. PLA70NC5, f. PLA70MC5, g. PLA30, h. PLA30NC5, i. PLA30MC5.

PLA and PBAT co-continuous phases increased after the addition of nano-$CaCO_3$, indicating nano-$CaCO_3$ made PLA crystal more complete in PLA70NC5. In addition, the temperature of the cold crystalline of PLA (T_{ccPLA}) in PLA70 increased after the addition of nano-$CaCO_3$, revealing the strong interaction between nano-$CaCO_3$ and PLA in PLA70NC5. Although it was relatively weak as shown in Figure 1a, the melting endothermic peak of PBAT was identified in the heating DSC scans of PLA30, PLA30NC5, and PLA30MC5. The melting temperature of PBAT (T_{mPBAT}) in PLA30NC5 was highest as shown in Figure 1b, indicating that the presence of nano-$CaCO_3$ was beneficial to the crystallization of PBAT in the composite.

The parameters derived from the cooling DSC scans of the PLA/PBAT/$CaCO_3$ composites in Figure 1c are shown in Figure 1d. During cooling at $-20°C·min^{-1}$, PLA90, PLA90MC5, and PLA30 showed a double-crystallization exothermic process, while PLA90NC5 and PLA70NC5 did not have any crystallization exothermic process, and PLA70, PLA70MC5, PLA30NC5, and PLA30MC5 had only a single-crystallization exothermic process. All the exothermic processes were attributed to the occurrence of PLA crystallization. In fact, PLA crystallized at high temperatures to form perfect crystals and at low temperatures to form imperfect crystals (9,30,31). $CaCO_3$ particles affected the crystallization of PLA from two aspects, namely, nucleation and cross-linking. Nano-$CaCO_3$ particles had a strong nucleation effect and tended to promote PLA crystallization at high temperature. However, the stronger cross-linking blocked the movement of PLA molecular chain segments and reduced the crystallization rate. This cross-linking reduced the movement of PLA molecular chains in PLA90NC5, making them completely less capable of cooling at a rate of $-20°C·min^{-1}$ without exothermic crystallization during the cooling process. So, PLA in PLA90NC5 did not crystallize as that in PLA90. However, the heterogeneous nucleation and cross-linking of micro-$CaCO_3$ were weaker than that of nano-$CaCO_3$ due to the small specific surface area and fewer active sites. So, PLA in PLA90MC5 crystallized as that in PLA90. Only one crystallization process occurred in PLA70 owing to the hindrance of PBAT to PLA through the large contact area caused by the bi-continuous phase of PLA and PBAT. PLA crystallization was retarded by nano-$CaCO_3$ particles in PLA70NC5. But micro-$CaCO_3$ particles had weak nucleation and cross-linking effects, so PLA in PLA70MC5 behaved like that in PLA70 as shown in Figure 1c. Unlike that in PLA90NC5 and PLA70NC5, PLA in PLA30NC5 crystallized as shown in Figure 1c, although it crystallized only at low temperature.

The parameters derived from the second heating DSC scans of the PLA/PBAT/$CaCO_3$ composites in Figure 1e are shown in Figure 1f. PLA90NC5 and PLA70NC5 had the cold crystallization process during the second heating, indicating that PLA chain arrangement was too slow to crystallize in the cooling circle at the rate of $-20°C·min^{-1}$. The occurrence of the cold crystallization in PLA90 showed an insufficient crystallization of PLA in the cooling circle at the rate of $-20°C·min^{-1}$, as shown in Figure 1c. In addition, nano-$CaCO_3$ increased the melting temperature of PBAT (T_{mPBAT}) in PLA30NC5.

3.2 Non-isothermal crystallization in neat PLA/PBAT blends and their composites containing micro-$CaCO_3$ fillers

In order to further describe the crystallization in the composites, the non-isothermal method was used based on the DSC scans. The cooling rate was set at −4, −6, −8, and $-10°C·min^{-1}$ after melting. The DSC scans are presented in Figure 2. X_t vs time is shown in Figure 3. Here X_t was defined as X_c at time t. The characteristic parameters coming from the scans in Figures 2 and 3 are listed in Figure 2e. The half time of crystallization, $t_{1/2}$, was defined as the time required to reach 50% of the final crystallinity.

Two crystallization exotherms occurred in PLA90, PLA90MC5, and PLA30 during cooling at the cooling rates of −4, −6, −8, and $-10°C·min^{-1}$. The exotherm at the high temperature was attributed to the formation of the perfect crystalline of PLA, and the other at the low temperature was attributed to the unperfect crystalline of PLA. In contrast, PLA70 and PLA70MC5 underwent only one crystallization exotherm occurring at the temperature between the two temperatures as shown in Figure 2, owing to a large contact area caused by the bi-continuous phase of PLA and PBAT. PLA30MC5 had two exothermic peaks at the cooling rate of $-4°C·min^{-1}$ but had one at the cooling rates of −6, −8, and $-10°C·min^{-1}$, as shown in Figure 2, which showed that PLA did not form perfect crystal when cooling at high rate.

As shown in Figures 2e and 3, $t_{1/2}$ decreased as the cooling rate increased, indicating an increase in the rate of crystallization. In addition, the crystallization temperature of PLA in PLA30 and PLA30MC5 rose as the cooling rate increased, and the crystallization speed increased.

3.3 Jeziorny method

The crystallization behavior was further investigated by the Jeziorny method. The isothermal crystallization

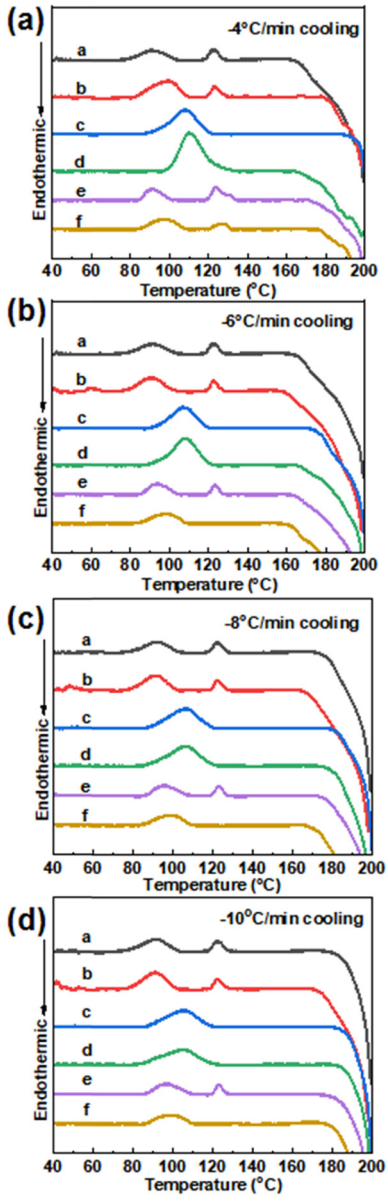

(e)

	Φ (°C/min)	T_c' (°C)	$t_{1/2}'$ (second)	T_c (°C)
a	-4	91.3	194	122.3
	-6	91.3	197	122.2
	-8	91.8	191	122.4
	-10	91.4	189	122.3
b	-4	99.8	225	122.9
	-6	90.6	133	122.7
	-8	91.5	93	122.3
	-10	91.3	69	122.3
c	-4	108	264	
	-6	107	168	
	-8	106	126	
	-10	106	102	
d	-4	110	432	
	-6	108	150	
	-8	107	126	
	-10	105	123	
e	-4	91.2	149	123.8
	-6	93.5	118	123.3
	-8	95.5	97	123.1
	-10	96.9	78	123.1
f	-4	97.7	196	126.9
	-6	98.7	130	
	-8	99.2	94	
	-10	99.8	80	

Figure 2: DSC curves of PLA/PBAT and their composites with micro-$CaCO_3$ fillers cooling at (a) −4°C·min^{-1}, (b) −6°C·min^{-1}, (c) −8°C·min^{-1}, and (d) −10°C·min^{-1}, and derived parameters (e). a–f presented in each of the subfigures (a–e) stand for a. PLA90, b. PLA90MC5, c. PLA70, d. PLA70MC5, e. PLA30, f. PLA30MC5.

kinetics is extensively described by the Avrami model (21), where X_t is expressed as follows:

$$1 - X_t = \exp(-Z_t t^n) \tag{3}$$

where n is the Avrami crystallization exponent, which depends on the nucleation mechanism and growth size; t is the crystallization time; and Z_t is the crystallization rate constant, which depends on nucleation and crystal growth. The linear form of the previous equation is as follows:

$$\ln[-\ln(1 - X_t)] = \ln Z_t + n\ln t \tag{4}$$

However, the temperature in non-isothermal crystallization is variable, and both nucleation and crystal growth are temperature dependent, so the Avrami model is not applicable to non-isothermal crystallization. In order to apply the Avrami model to non-isothermal crystallization, Jeziorny proposed that Z_t is influenced by the cooling rate (φ) and verified by having a cooling rate term as shown in Eq. 5 below (20).

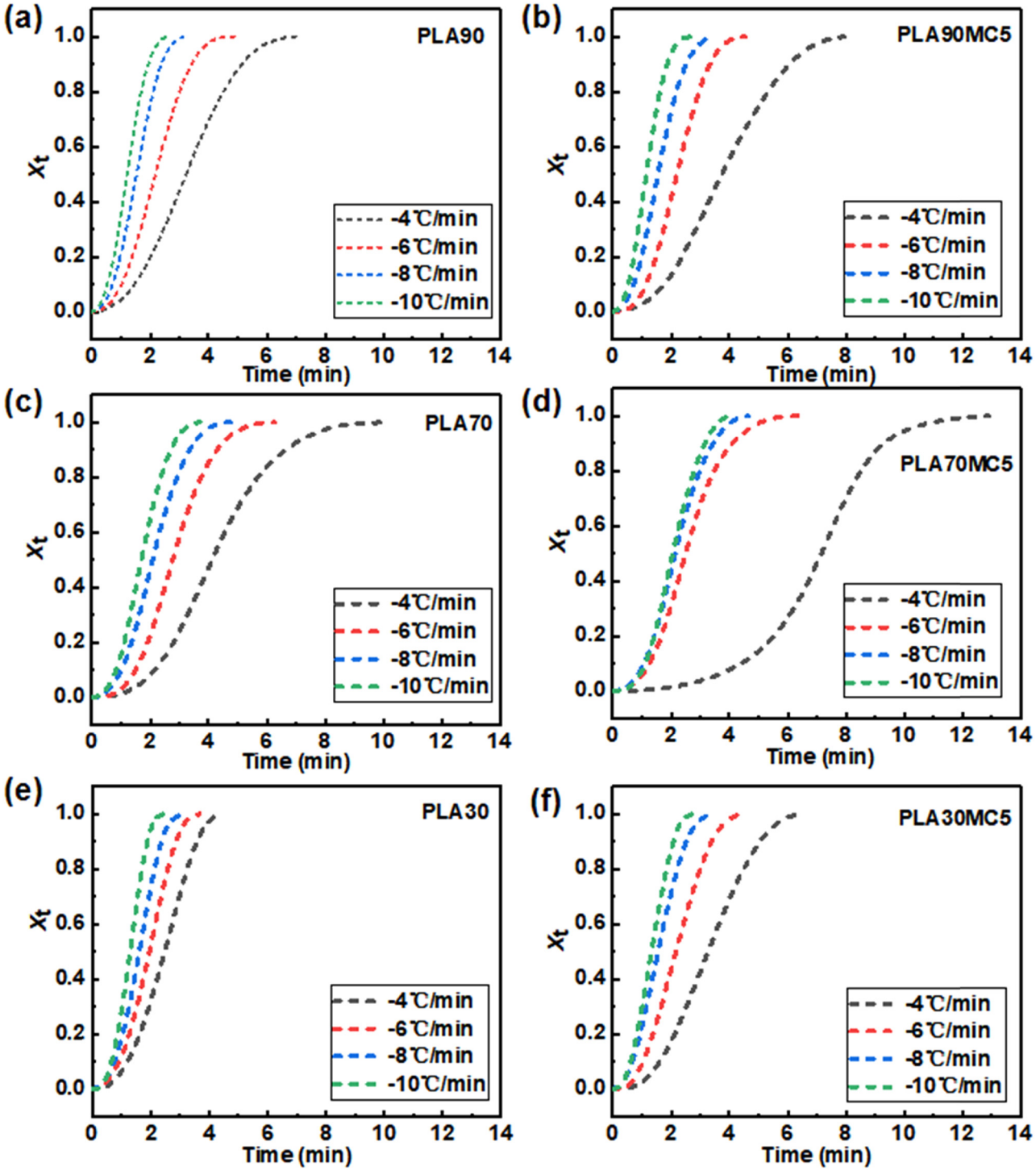

Figure 3: Plots of X_t of crystallization vs time at cooling rates of −4, −6, −8, and −10°C·min^{-1} for: (a) PLA90, (b) PLA90MC5, (c) PLA70, (d) PLA70MC5, (e) PLA30, and (f) PLA30MC5.

$$\ln(Z_c) = \ln(Z_t)/\varphi \quad (5)$$

where Z_c is the corrected Jeziorny crystallization constant. According to Eq. 4, n and Z_t in the present study were obtained from the slope and intercept of the curve between $\ln[-\ln(1 - X_t)]$ and $\ln t$ shown in Figure 4. Then, the value of Z_c was calculated by Eq. 3. n and Z_c values of the composites were listed in Table 3.

Despite the different continuous phases in PLA/PBAT/$CaCO_3$ listed in Table 3, the n values of the composites were close to each other as shown in the table, indicating

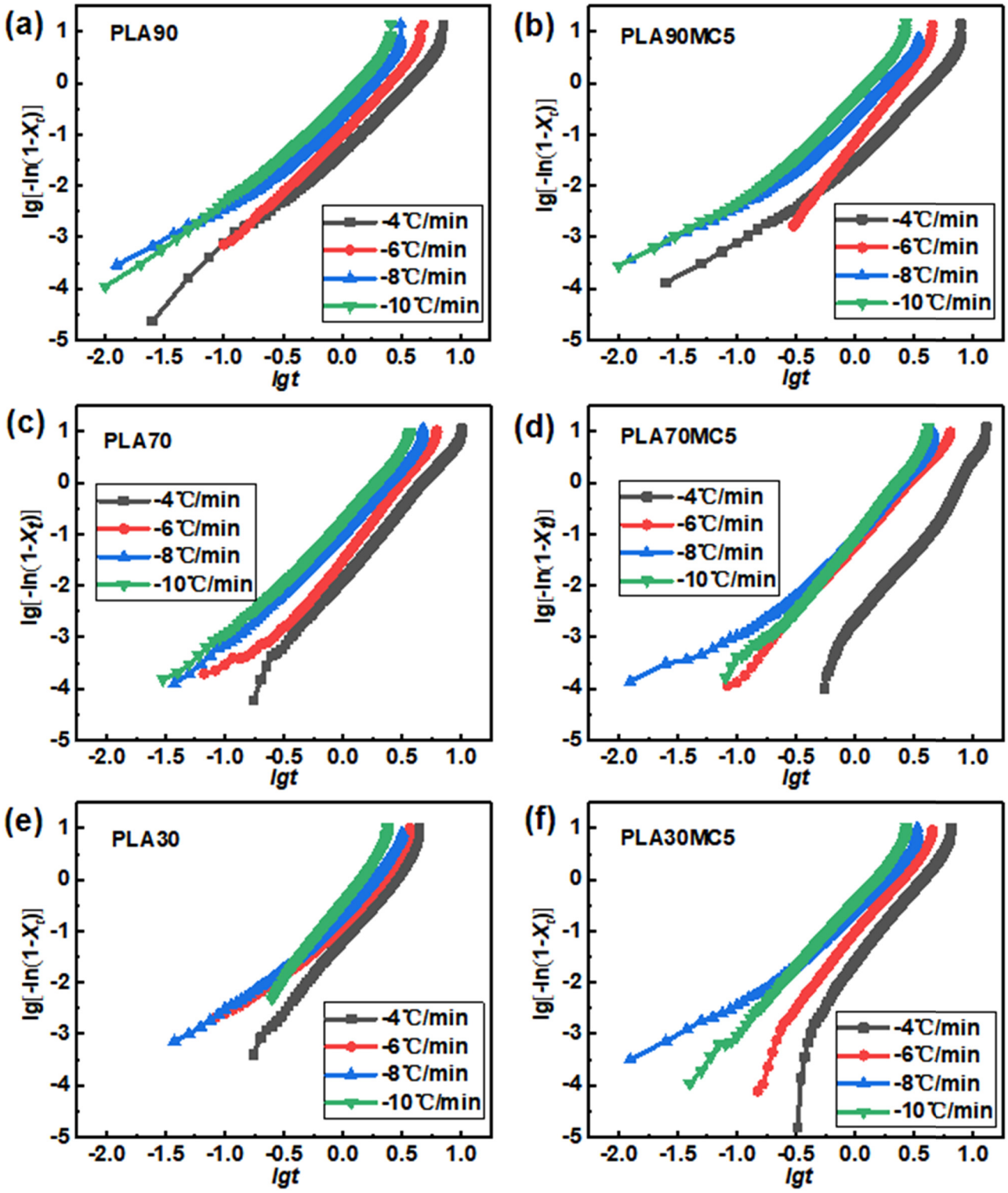

Figure 4: Avrami plots for: (a) PLA90, (b) PLA90MC5, (c) PLA70, (d) PLA70MC5, (e) PLA30, and (f) PLA30MC5.

a similar nucleation mechanism. As for the crystallization rate, Z_c of each of the composites almost always increased significantly as the cooling rate increased. An increase in Z_c implied an increase in the crystallization rate with an increase in the cooling rate, which was consistent with the parameters in Figure 2e.

3.4 Mo method

Ozawa's model was used to describe non-isothermal crystallization as a development of the Avrami model by assuming that the non-isothermal crystallization process was a small step in isothermal crystallization. The fractional crystallinity (X_t) for time t is shown in Eq. 6 as follows:

$$X_t = [1 - \exp(-K_0^m/\varphi)] \quad (6)$$

The linear form of this equation was more commonly used as follows:

$$\ln[-\ln(1 - X_t)] = \ln(K_0) - m\ln(\varphi) \quad (7)$$

where m and K_0 were obtained from the slope and interception on the y-axis of the graph from the relationship between $\ln[-\ln(1 - X_t)]$ and $\ln(\varphi)$, respectively.

Mo's method combined Avrami and Ozawa equations to describe non-isothermal crystallization process. Mo equation is as follows:

$$\ln\varphi = \ln F(T) - \gamma\ln(t) \quad (8)$$

where $F(T)$ was the modified parameter of the crystallization rate and γ was the ratio of n to m in the Avrami equation and the Ozawa equation, respectively, which was related to the crystallization dimension. A series of straight lines were drawn in Figure 5 in the case of a given value of relative crystallinity. $F(T)$ and γ were obtained from the intercepts and slopes of the straight lines in Figure 5. The parameters obtained from the $\ln\varphi$ vs $\ln t$ relationship plots are given in Table 4 for each sample in Figure 5. All plots show good linearity, which indicated that Mo's method was suitable for describing the non-isothermal crystallization kinetics in this study although the continuous phases in the composites were different.

$F(T)$ increased with the increase in X_t for each composite as shown in Table 4, indicating that the faster the cooling rate, the higher the crystallinity obtained per unit of crystallization time in all the PLA/PBAT/$CaCO_3$ composites. The values of $F(T)$ of PLA30 and PLA30MC5 were significantly higher than others, which revealed that the crystallization rate of PBAT in PLA30 and PLA30MC5 was very fast. Moreover, the a value increased significantly with increasing X_t, indicating an increase in the size of grain growth during non-uniform nucleation of PLA. In other words, the achievement of higher X_t required faster cooling rate and increased crystalline dimension in these composites.

Table 3: Jeziorny parameters of non-isothermal crystallization in the PLA/PBAT/$CaCO_3$ composites

Samples	Φ (°C·min^{-1})	n	Average n	lg Z_t/Φ	Z_c	r^2
PLA90	−4	2.29	2.28	−1.26	0.055	0.9869
	−6	2.46		−0.94	0.115	0.9917
	−8	2.18		−0.50	0.316	0.9698
	−10	2.20		−0.27	0.537	0.9830
PLA90MC5	−4	2.23	2.41	−1.39	0.041	0.9775
	−6	3.07		−1.20	0.063	0.9953
	−8	2.14		−0.52	0.302	0.9761
	−10	2.21		−0.23	0.589	0.9767
PLA70	−4	2.72	2.62	−1.86	0.34	0.9987
	−6	2.78		−1.40	0.58	0.9920
	−8	2.49		−0.92	0.77	0.9931
	−10	2.48		−0.69	0.85	0.9901
PLA70MC5	−4	3.34	2.80	−2.94	0.18	0.9876
	−6	2.60		−1.22	0.63	0.9991
	−8	2.36		−0.91	0.77	0.9777
	−10	2.88		−1.05	0.79	0.9930
PLA30	−4	2.83	2.66	−1.20	0.50	0.9930
	−6	2.39		−0.76	0.75	0.9699
	−8	2.36		−0.55	0.85	0.9738
	−10	3.06		−0.45	0.90	0.9934
PLA30MC5	−4	3.04	2.65	−1.71	0.37	0.9830
	−6	2.86		−1.10	0.66	0.9927
	−8	2.11		−0.50	0.87	0.9778
	−10	2.60		−0.43	0.91	0.9955

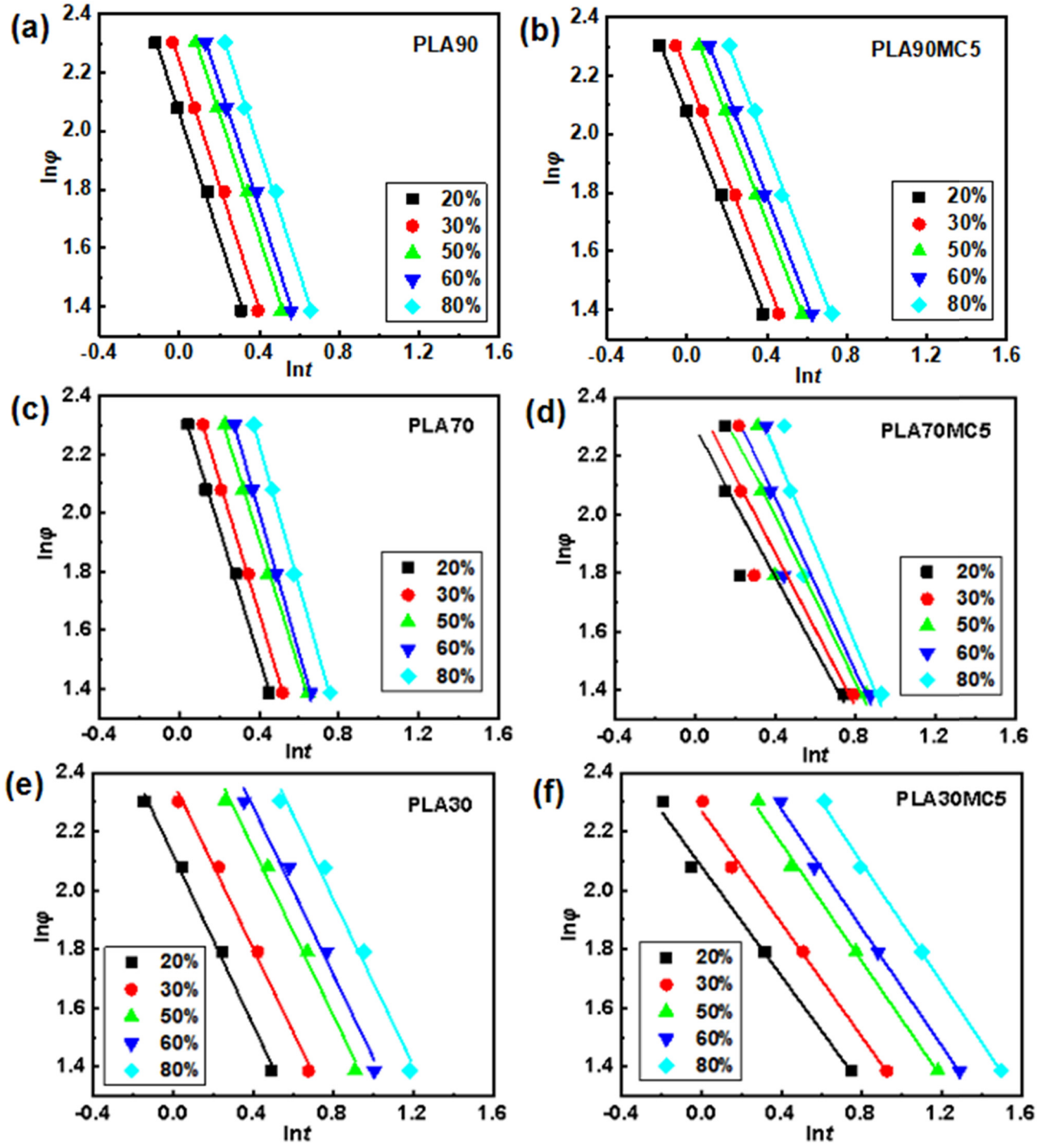

Figure 5: Plots of lg φ vs lg t for the cold crystallization of: (a) PLA90, (b) PLA90MC5, (c) PLA70, (d) PLA70MC5, (e) PLA30, and (f) PLA30MC5.

3.5 Mechanical behavior of the PLA/PBAT/$CaCO_3$ composites

The experimental results for tensile performance and impact strength of the PLA/PBAT/$CaCO_3$ composites in the study are shown in Figure 6.

PLA90MC5 exhibited the highest tensile strength among all the composites as shown in Figure 6, which showed that five parts of nano-$CaCO_3$ enhanced PLA90 with PLA as a single continuous phase more effectively than PLA70 with PLA and PBAT as co-continuous phases and PLA30 with PBAT as a single continuous phase. The tensile strength of

Table 4: Mo's parameters for the crystallization of PLA90, PLA90MC5, PLA70, PLA70MC5, PLA30, and PLA30MC5

Samples	X_t (%)	$F(T)$	a	r^2
PLA90	20	2.44	0.92	0.9944
	30	2.64	0.92	0.9955
	50	2.94	0.92	0.9964
	60	3.07	0.92	0.9968
	80	3.35	0.92	0.9971
PLA90MC5	20	2.46	0.77	0.9966
	30	2.61	0.77	0.9989
	50	2.85	0.78	0.9995
	60	2.96	0.78	0.9988
	80	3.19	0.78	0.9943
PLA70	20	2.83	0.97	0.9959
	30	3.05	0.99	0.9988
	50	3.36	0.95	0.9965
	60	3.62	1.04	0.9996
	80	4.01	1.05	0.9974
PLA70MC5	20	2.70	0.54	0.7132
	30	2.82	0.56	0.7293
	50	3.04	0.61	0.7536
	60	3.16	0.64	0.7626
	80	3.47	0.71	0.7935
PLA30	20	8.32	1.45	0.9926
	30	10.69	1.42	0.9901
	50	14.99	1.41	0.9827
	60	17.28	1.42	0.9778
	80	22.27	0.75	0.7372
PLA30MC5	20	8.01	0.93	0.9856
	30	9.68	0.96	0.9878
	50	12.88	0.99	0.9936
	60	14.51	1.00	0.9951
	80	18.36	1.02	0.9972

the PLA70MC5 was higher than that of PLA70NC5, which showed that five parts of micro-$CaCO_3$ was more effective than five parts of nano-$CaCO_3$ in enhancing PLA70 with PLA and PBAT co-continuous phases.

The yield strength of PLA70 was higher than that of PLA90 and PLA30, and it became higher after adding $CaCO_3$. In addition, the yield strength of PLA70MC5 was higher than that of PLA70NC5.

The high elongation at break of PLA30 and the composites containing $CaCO_3$ was attributed to the fact that PBAT acted as a continuous phase and PLA as a dispersed phase in these composites, thus exhibiting more PBAT-like properties. Moreover, the elongations at break of PLA30NC5 and PLA30MC5 were much higher than that of PLA30.

PLA30 had the lowest impact strength in the composites in the study but was significantly toughened by the addition of $CaCO_3$. The impact strengths of PLA30NC5 and PLA30MC5 were much higher than that of the corresponding composites containing nano-$CaCO_3$ and micro-$CaCO_3$ as shown in Figure 6.

3.6 Cross-sectional micromorphology

To analyze the morphology of PLA/PBAT/$CaCO_3$ composites further, SEM was used. The SEM images of fracture surfaces of the composites from the tensile testing are shown in Figure 7.

As a dispersed phase, PBAT was not independent in PLA90, resulting in insufficient identification from Figure 7a. Figure 7b showed a coarse fracture surface with exposed individual and aggregated nano-$CaCO_3$ particles, which showed that the $CaCO_3$ filler had poor compatibility with PLA and was not completely coated by PLA in PLA90NC5. In Figure 7c, completely exposed micro-$CaCO_3$ particles were observed, which indicated that micro-$CaCO_3$ was obviously separated from the matrix of PLA in PLA90MC5.

As shown in Figure 7d, the fracture surface displayed flaky protrusions of PBAT, which was obviously different from that in Figure 7a. The interfaces between PLA and PBAT phases were not obviously separated on the cross section, indicating that PLA and PBAT had certain compatibility in PLA70, owing to a large contact area caused by the bi-continuous phase of PLA and PBAT. The formation of PBAT flakes was due to the low PBAT content in PLA70 and a much lower yield stress than PLA, thus underwent plastic deformation at a lower stress than PLA. A rough fracture surface with exposed nano-$CaCO_3$ particles was observed in Figure 7e. The fracture surface of PLA70MC5 as shown in Figure 7f was close to that shown in Figure 7d, indicating that micro-$CaCO_3$ had little effect on the micro morphology of the composite.

Figure 7g displayed a fracture surface with dispersed PLA grains, which showed poor compatibility between PLA and PBAT in PLA30. But the PLA grains are difficult to observe in Figure 7h with a small amount of exposed nano-$CaCO_3$ particles, which displayed the enhanced compatibility between PLA and PBAT in PLA30NC5 by nano-$CaCO_3$ particles. More independent grains of PLA were observed in Figure 7i, which showed poor compatibility between PLA and PBAT in PLA30MC5.

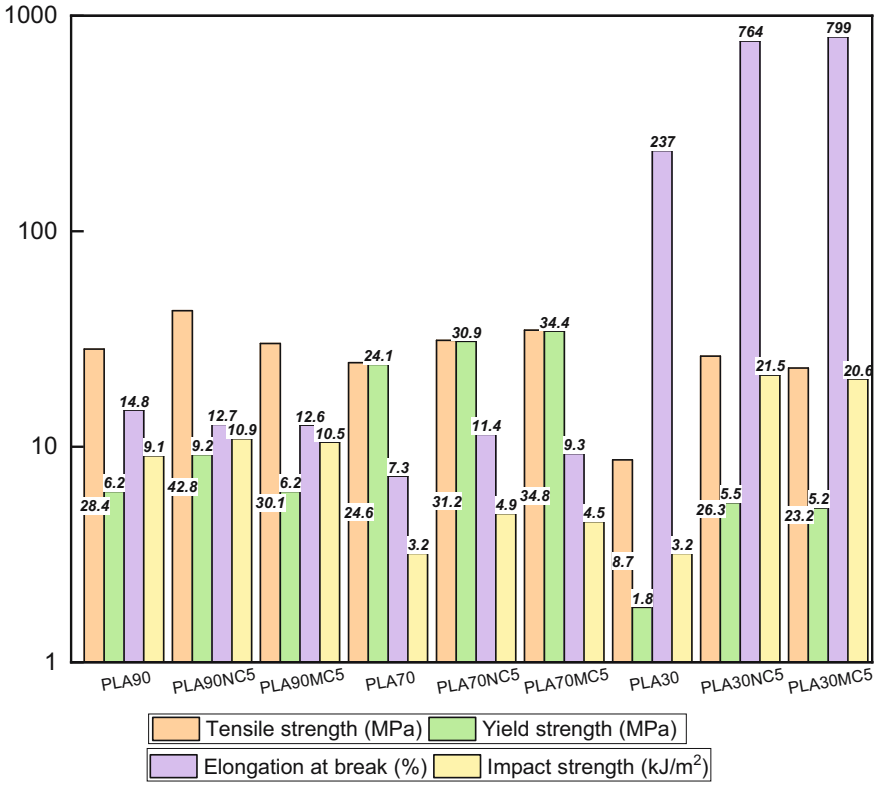

Figure 6: Experimental results for tensile strength, yield strength, elongation at break of composites, and impact strength.

4 Conclusion

PLA crystallization was related to PLA and PBAT ratio, cooling rates, and $CaCO_3$ filler in PLA/PBAT/$CaCO_3$ composites. In PLA90 and PLA30, PLA formed perfect crystals at high temperature and imperfect crystals at low temperature. In PLA70, PLA did not form perfect crystals due to the large contact area between PLA and PBAT in the bi-continuous phase. The $CaCO_3$ filler acted as both a heterogeneous nucleation agent in PLA crystallization and a cross-linking agent of PLA molecular chains in PLA/PBAT/$CaCO_3$ composites. Nano-$CaCO_3$ had a strong cross-linking effect in PLA phase in PLA90NC5 and PLA70NC5, blocking PLA crystallization during rapid cooling. However, due to the dominant dispersion of nano-$CaCO_3$ in PBAT continuous phase in PLA30NC5, the nano-$CaCO_3$ cross-linking in PLA phase was weakened, and PLA still crystallized even at a rapid cooling rate. Micro-$CaCO_3$ had a weaker cross-linking effect on PLA molecular chains than nano-$CaCO_3$ owing to low specific surface area, so PLA crystallized in PLA90MC5, PLA70MC5, and PLA30MC5 regardless of the cooling rate. Nevertheless, PLA in the composites was similar in the crystallization growth pattern regardless of the continuous phase, which was revealed by Jeziorny method. In addition, Mo method displayed that the PLA crystallization rate in PLA30 and PLA30MC5 was faster than that in other composites.

The $CaCO_3$ filler slightly increases the mechanical properties of PLA90 and PLA70, but improved that of PLA30 by several times regardless of the particle size of the filler, which was attributed to the tendency of the $CaCO_3$ filler to be predominantly dispersed in the PBAT continuous phase. Nano-$CaCO_3$ was easy to aggregate in PLA90NC5 and PLA70NC5, but not in PLA30NC5, which may be the reason for the excellent mechanical properties of PLA30NC5 compared with PLA30. In other words, the filler only reduced the material cost of PLA90 and PLA70, and the filler not only reduced the material cost of PLA30, but also improved its mechanical properties.

Funding information: This study was supported by the Provincial Scientific Project of Henan (Grant 172102210228), the Innovation Fund of Henan Hairuixiang Technology Co., Ltd (Grant 2021001), and the Henan Province Science and Technology Research Project (Grant 232102230097).

Author contributions: Weiqiang Song: conceptualization, supervision, writing – original draft, and writing – review and editing; Zhenyu Guo: validation, formal analysis, investigation, and data curation; Xueqin Wei: project

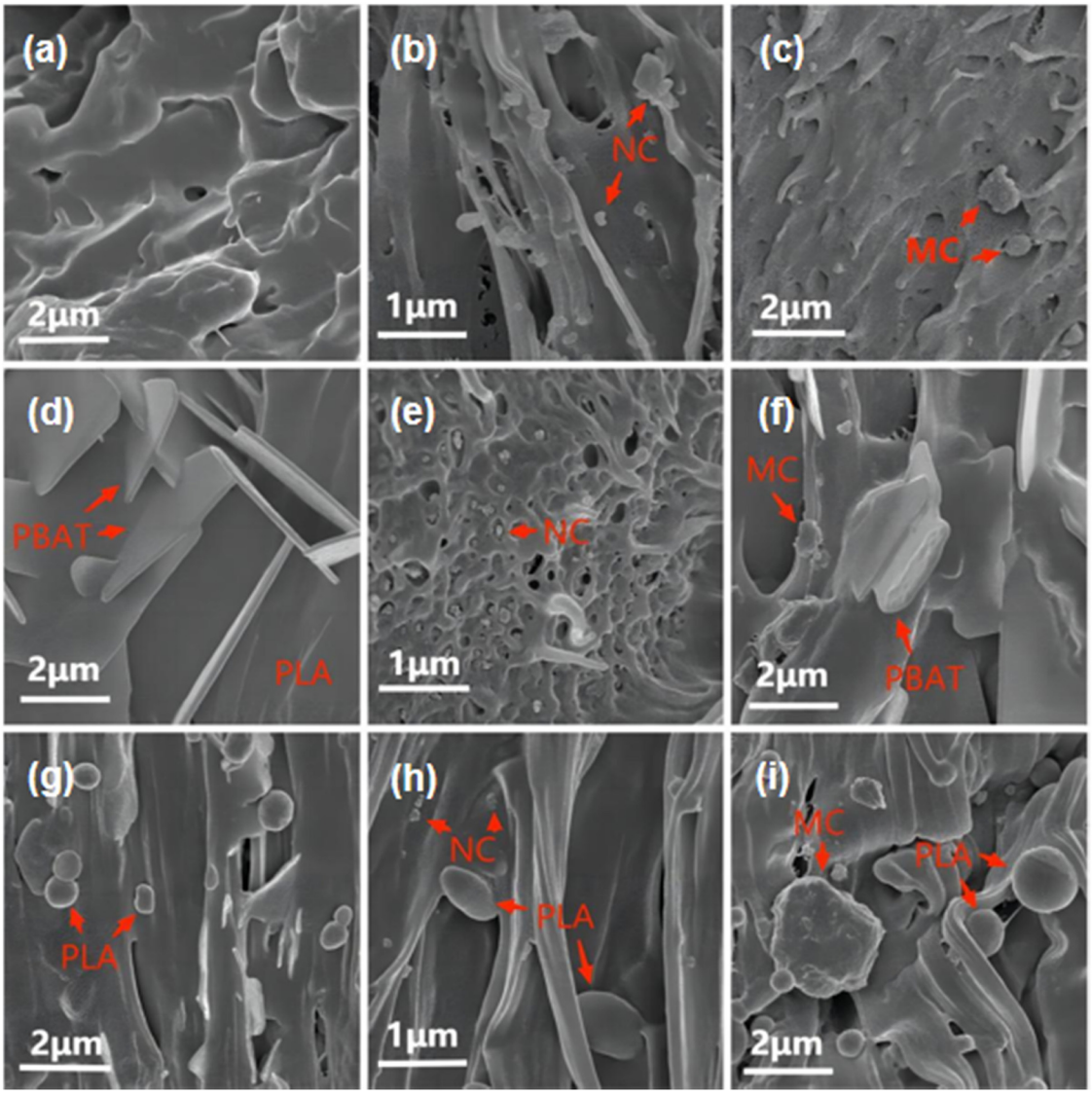

Figure 7: Scanning electron micrographs of fracture surfaces of: (a) PLA90, (b) PLA90NC5, (c) PLA90MC5, (d) PLA70, (e) PLA70NC5, (f) PLA70MC5, (g) PLA30, (h) PLA30NC5, and (i) PLA30MC5.

administration and supervision; Yu Feng: formal analysis and project administration; Yixuan Song: investigation and software; Zidong Guo: investigation and software; Wenxi Cheng: project administration and supervision; Wei Miao: project administration and supervision; Bo Cheng: project administration and supervision; Shiping Song: project administration and supervision.

Conflict of interest: The authors state no conflict of interest.

Data availability statement: All data for the manuscript are available upon request.

References

(1) Zhang Y, Ma J, O'Connor P, Zhu YG. Microbial communities on biodegradable plastics under different fertilization practices in farmland soil microcosms. Sci Total Environ. 2022;809:152184.

(2) Schettini E, Scarascia-Mugnozza G, Blanco I, Convertino F, Vox G. 12-Agricultural plastic waste. Woodhead publishing series in civil and structural engineering, Handbook of sustainable concrete and industrial waste management. Cambridge: Woodhead Publishing; 2022. p. 255–68.

(3) D'amico DA, Iglesias Montes ML, Manfredi LB, Cyras VP. Fully bio-based and biodegradable polylactic acid/poly(3-hydroxybutirate) blends: Use of a common plasticizer as performance improvement strategy. Polym Test. 2016;4922–28.

(4) Rincón-Iglesias M, Salado M, Lanceros-Mendez S, Lizundia E. Magnetically active nanocomposites based on biodegradable polylactide, polycaprolactone, polybutylene succinate and polybutylene adipate terephthalate. Polymer. 2022;249:124804.
(5) Razavi M, Wang SQ. Why is crystalline poly (lactic acid) brittle at room temperature? Macromolecules. 2019;52(14):5429–41.
(6) Jia SL, Zhao L, Wang XY, Chen YJ, Pan HW, Han LJ, et al. Poly (lactic acid) blends with excellent low temperature toughness: A comparative study on poly (lactic acid) blends with different toughening agents. Int J Biol Macromol. 2022;201(15):662–75.
(7) Martin O, Avérous L. Poly (lactic acid): Plasticization and properties of biodegradable multiphase systems. Polymer. 2001;42:6209–19.
(8) Shen S. Compatibilization, processing and characterization of poly (butylene adipate terephthalate)/polylactide (PBAT/PLA) blends. Mater Res Express. 2022;9:025308; Saeidlou S, Huneault MA, Li HB, Park CB. Poly (lactic acid) crystallization. Prog Polym Sci. 2012;37(12):1657.
(9) Li GZ, Xia Y, Mu GQ, Yang Q, Zhou HM, Lin XJ, et al. Phase structure analysis and composition optimization of poly (lactic acid)/poly(butylene adipate-co-terephthalate) blends. J Macromol Sci Part B. 2022;61(3):413–24.
(10) Li K, Peng J, Turng L-S, Huang HX. Dynamic rheological behavior and morphology of polylactide/poly (butylenes adipate-co-terephthalate) blends with various composition ratios. Adv Polym Technol. 2011;30(2):150–7.
(11) Gill YQ, Mehdi S, Mehmood U. Enhancement of polylactide/poly (butylene adipate-co-terephthalate) blend [ECOVIO] properties by carboxylated nitrile butadiene rubber (XNBR) addition for smart packaging applications. Mater Lett. 2022;306:130881.
(12) Sun DX, Gu T, Qi XD, Yang JH. Highly-toughened biodegradable poly (L-lactic acid) composites with heat resistance and mechanical-damage-healing ability by adding poly(butylene adipate-co-butylene terephthalate) and carbon nanofibers. Chem Eng J. 2021;424:130558.
(13) Deng YX, Yu CY, Wongwiwattana P, Thomas NL. Optimising ductility of poly (Lactic Acid)/Poly (Butylene Adipate-co-Terephthalate) blends through co-continuous phase morphology. J Polym Environ. 2018;26:3802–16.
(14) Clizia A, Massimiliano B. Addition of thermoplastic starch (TPS) to binary blends of poly (lactic acid) (PLA) with poly (butylene adipate-co-terephthalate) (PBAT): Extrusion compounding, cast extrusion and thermoforming of home compostable materials. Chin J Polym Sci. 2022;40(10):1269–86.
(15) Gui H, Zhao MY, Zhang SQ, Yin RY. Active antioxidant packaging from essential oils incorporated polylactic acid/poly (butylene adipate-co-terephthalate)/thermoplastic starch for preserving straw mushroom. Foods. 2022;11(15):2252.
(16) Aragón-Gutierrez A, Arrieta MP, López-González M, Fernández-García M, López D. Hybrid biocomposites based on poly (lactic acid) and silica aerogel for food packaging applications. Materials. 2020;13(21):4910.
(17) Alakrach AM, Al-Rashdi AA, Al-Omar MK, Jassam TM. Physical and barrier properties of polylactic acid/halloysite nanotubes-titanium dioxide nanocomposites. Mater Sci Forum. 2021;1021:280–9.
(18) Sanusi OM, Benelfellah A, Papadopoulos L, Terzopoulou Z. Properties of poly(lactic acid)/montmorillonite/carbon nanotubes nanocomposites: Determination of percolation threshold. J Mater Sci. 2021;56:16887–901.
(19) Jalali A, Huneault MA, Elkoun S. Effect of thermal history on nucleation and crystallization of poly (lactic acid). J Mater Sci. 2016;51(16):7768–79.
(20) Shi N, Dou Q. Non-isothermal cold crystallization kinetics of poly (lactic acid)/poly (butylene adipate-co-terephthalate)/treated calcium carbonate composites. J Therm Anal Calorim. 2015;119(1):635–42.
(21) Deetuam C, Samthong C, Choksriwichit S, Somwangthanaroj A. Isothermal cold crystallization kinetics and properties of thermoformed poly (lactic acid) composites: effects of talc, calcium carbonate, cassava starch and silane coupling agents. Iran Polym J. 2020;19(2):103–16.
(22) Rocha DB, de Carvalho JS, de Oliveira SA, Rose DDS. A new approach for flexible PBAT/PLA/CaCO3 films into agriculture. J Appl Polym Sci. 2018;135(35):46660.
(23) Han LJ, Han CY, Bian JJ, Bian YJ. Preparation and characteristics of a novel nano-sized calcium carbonate (nano-$CaCO_3$)-supported nucleating agent of poly(L-lactide). Polym Eng & Sci. 2012;52(7):1474–84.
(24) Nekhamanurak B, Patanathabutr P, Hongsriphan N. The influence of micro-/nano-$CaCO_3$ on thermal stability and melt rheology behavior of poly (lactic acid). Energy Procedia. 2014;56:118–28.
(25) Mulla MZ, Rahman MRT, Marcos B, Tiwari B. Poly lactic acid (PLA) nanocomposites: Effect of inorganic nanoparticles reinforcement on its performance and food packaging applications. Molecules. 2021;26(7):1967.
(26) Gao C, Guo J, Xie H. The effect of alginate on the mechanical, thermal, and rheological properties of nano calcium carbonate-filled polylactic acid composites. Polym Eng Sci. 2019;59(9):1882–8.
(27) Chen L, Dou Q. Influence of the combination of nucleating agent and plasticizer on the non-isothermal crystallization kinetics and activation energies of poly (lactic acid). J Therm Anal Calorim. 2020;139(2):1069–90.
(28) Lee JM, Hong JS, Ahn KH. Particle percolation in a poly (lactic acid)/calcium carbonate nanocomposite with a small amount of a secondary phase and its influence on the mechanical properties. Polym Compos. 2019;40(10):4023–32.
(29) Song Q. Thermal and mechanical properties of poly(lactic acid)/poly(butylene adipate-co-terephthalate)/calcium carbonate composite with single continuous morphology. e-polymers. 2022;22:1007–20.
(30) Zhang JM, Tashiro K, Tsuji H, Domb AJ. Disorder-to-order phase transition and multiple melting behavior of poly(l-lactide) investigated by simultaneous measurements of WAXD and DSC. Macromolecules. 2008;41(4):1352–7.
(31) Kawai T, Rahman N, Matsuba G. Crystallization and melting behavior of poly (l-lactic acid). Macromolecules. 2007;40(26):9463–9.